Journal of
Ceramic Science
and Technology

J. Ceram. Sci. Technol. , **08** [3] 421-432 (2017)
DOI: 10.4416/JCST2017-00065
available online at: http://www.ceramic-science.com

Methods for Geopolymer Formulation Development and Microstructural Analysis

A. van Riessen[1], W.D.A. Rickard[*1], R.P. Williams[1], G.A. van Riessen[2]

[1]John de Laeter Centre, Curtin University, Perth, Western Australia
[2]Department of Chemistry and Physics, School of Molecular Sciences, La Trobe University, Melbourne, Victoria 3086, Australia

received July 31, 2017; received in revised form August 5, 2017; accepted August 21, 2017

Abstract

Alkali-activated materials (AAMs) and geopolymers have been extensively studied, although widespread commercialisation has been hampered, in part, by the use of precursors that are rarely homogeneous and are generally poorly characterised. Even when precursors are well characterised, their extent of reaction during geopolymer synthesis is not well known, leading to a disparity between targeted and actual compositional ratios. Small variations in compositional ratios, particularly Si:Al, can lead to dramatic changes in physical properties. A process for characterising precursors, focussing on their reactive component, will be described here, followed by methods that can be used to determine the extent of reaction in the final product. Characterising the final product is important, but it does not reveal what processes occur between mixing the precursors and setting of the solid geopolymer. We will also describe a method that can be used to track dissolution of precursors and subsequent evolution of the alkali-activated product, thus providing a more comprehensive picture of geopolymerisation. This paper demonstrates a link between precursor characterisation and the extent of reaction in order to provide those working with alkali-activated materials with additional knowledge enabling them to manufacture reproducible, high-quality products.

Keywords: Alkali-activated materials, geopolymer, precursor

I. Introduction

The study of alkali-activated binders has been ongoing for many years [1,2,3] and there are some examples of commercialisation appearing in the literature [4]. One of the obvious benefits of alkali-activated products is that their precursors are likely to be industrial by-products, leading to industrial sustainability and lower green-house gas emissions. However, the use of by-products is also a potential drawback as these precursors are generally not graded to a specific standard and are often compositionally inhomogeneous. For instance, fly ash can vary in composition and particle size according to source coal properties, level of grinding of the coal, the firing regime in the power station and any post-firing treatment such as size classification [5]. Not only can the overall composition of the fly ash vary but so can the reactive component that is utilised to make the geopolymer. One way to handle the variation in the fly ash is to adjust the mixing regime and formulation to match the fly ash after it is thoroughly characterised [6,7]. The Portland cement industry has been doing this successfully for many years [8] and thus similar practices also need to be adopted by those manufacturing geopolymers. Analogous assessments about homogeneity and characterisation can also be made about ground granulated blast furnace slag.

Adopting thorough analytical methods to characterise precursors for the manufacture of alkali-activated materials is necessary, but that in itself does not overcome all the challenges in manufacturing these materials. For instance, knowledge of the amount and composition of the reactive component in a precursor will enable a realistic and useful formulation to be determined; however, the extent of reaction of the reactive component is often unknown. For example, if the reactive component of fly ash is ensconced inside the ash spheres then the extent of reaction may be very low, whereas if it is present on the surface, the opposite may be true. Even the use of highly homogeneous metakaolin with low impurities will result in considerably less than 100 % extent of reaction [9]. Without accurate prediction of the extent of reaction, the amount of geopolymer binder and composition of the binder are unknown, leading to unpredictable outcomes in physical properties. The extent of reaction in geopolymers has been measured using a number of methods including x-ray diffraction [9] and nuclear magnetic resonance [10]. Generally alkali-activated formulations are based on a number of target ratios, for instance Si:Al, Na:Al, water:solid. Williams and van Riessen [6] used a novel approach based on matrices to generate weight fractions of precursors required based on targeted ratios. If only part of the precursor reacts, then the actual ratios will be different. This difference in target and actual ratios may be significant and is unacceptable in cases where mass production is envisaged. Scanning electron microscopy (SEM) and x-ray diffraction (XRD) techniques can be used to measure the critical composition-

* Corresponding author: w.rickard@curtin.edu.au

al ratios such as Si:Al and Na:Al and compare them with targeted values [9]. Where there is a significant difference, it is worth determining the cause so methods can be introduced to minimise these differences. For instance, a fly ash with a low extent of reaction may have the reactive component embedded inside the ash spheres so milling of the ash prior to mixing with alkali may be an effective solution. Even if the extent of reaction is high it may still be improved by milling [11].

Characterising precursors and final products is appropriate when targeted properties are being sought for specific applications, such as high strength for load-bearing products. However, it leaves open the question of how did the system evolve to the final product and can this information assist in optimising future product development? One way to track precursor dissolution and subsequent formation of geopolymer is the use of *in situ* high-speed XRD. An obvious way to achieve high-speed XRD is to use a high-brightness x-ray beam produced at a synchrotron [12]. XRD can then be conducted on a freshly combined precursor-alkali mix and repeat patterns collected every few minutes to track dissolution of the precursor and formation of the geopolymer. Liu *et al.* [13] successfully demonstrated the use of Bragg Coherent Diffraction to image a hydrating crystal of calcium monoaluminate over several days.

The schematic shown in Fig. 1 is an idealised view on how an unknown aluminosilicate might be characterised to allow a geopolymer formulation to be determined. Once the geopolymer is made, the important compositional ratios can be measured and compared with targeted values. If the two sets of ratios do not match, beneficiation of the precursor may need to be undertaken until target and actual ratios match. Finally, *in situ* measurements of dissolution and geopolymer formation rates should be performed and, if necessary, these rates should be optimised to match targeted product specifications. The following sections include a brief introduction to relevant analytical techniques and a number of case studies which highlight the importance of precursor characterisation and monitoring the extent of reaction.

II. Crystalline Phase Analysis using XRD

For many glassy and disordered (amorphous) materials the lack of long-range atom ordering does not result in sharp reflections but a broad amorphous hump in an XRD pattern. A typical x-ray diffractometer uses a fixed wavelength and moves the x-ray source from low- to high-incident angle while at the same time a detector is moved to measure the intensity of the scattered radiation. The outcome is a series of reflections versus reflection angle. If a number of reflections are measured for a particular phase then its identity can be determined from a database. This is the simplest way to use XRD, namely phase identification. If the sample is composed of many phases then their XRD patterns will likely overlap and software will be necessary to deconvolve the patterns before phase identification is possible (qualitative analysis). Once phases in the pattern have been identified then more sophisticated analysis software, based on the Rietveld method [14], can be used to extract considerably more information. Rietveld refinement is whole pattern analysis where users input crystallographic information for each phase (inorganic crystal structure database) and the software conducts a least

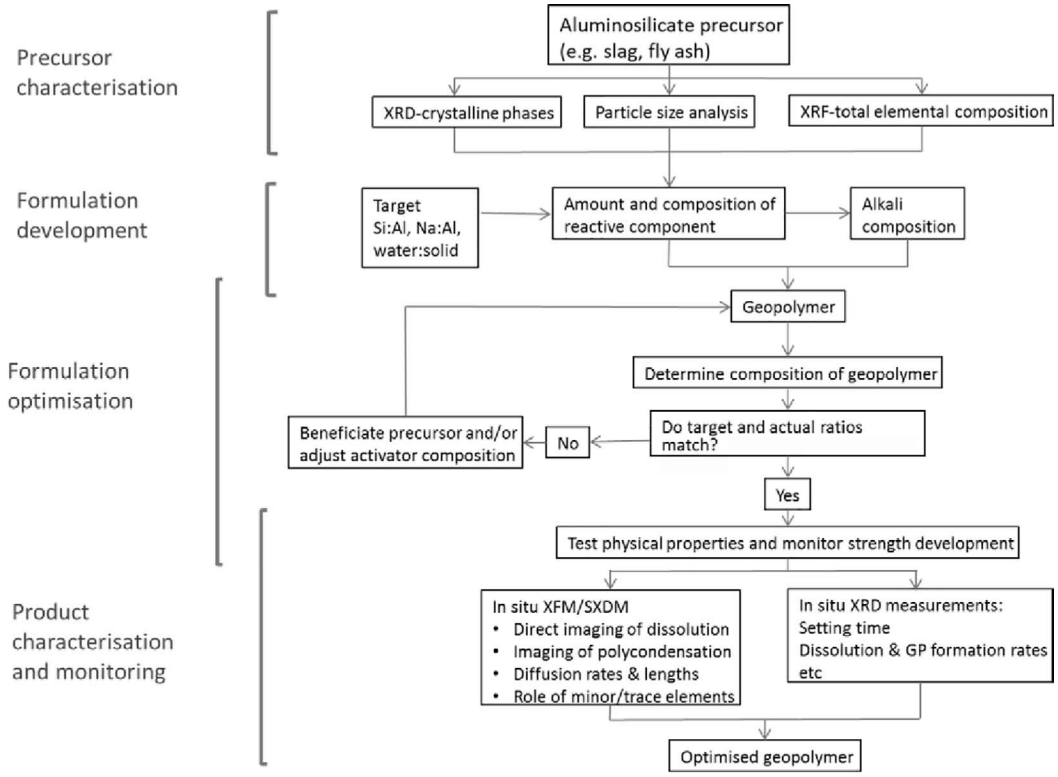

Fig. 1: Schematic showing proposed workflow for precursor assessment and geopolymer characterisation leading to optimisation. XRD=x-ray diffraction; XRF=x-ray fluorescence; XFM=x-ray fluorescence microscopy; SXDM= scanning x-ray diffraction microscopy.

squared refinement to calculate a pattern to match the measured pattern. Refinement with XRD data collected from a fully crystalline sample enables the amount of each phase to be calculated, resulting in quantitative phase analysis. Much more information can be discerned from the fitted pattern such as crystallite size, strain, etc. If quantitative analysis is required for a sample that has an amorphous component, then an internal standard can be added and the amount of amorphous material can also be obtained. The amorphous component can be treated as another phase and modelled using the approach of partial or no known crystal structure (PONKCS) [15]. This capability is important for alkali-activated materials as their microstructure typically includes amorphous unreacted precursor, amorphous geopolymer and several crystalline phases. Fortunately, the broad amorphous humps from unreacted precursor and amorphous geopolymer are different owing to variations in intensity and position. It is important to be able to differentiate between precursor and geopolymer so that the extent of reaction can be determined and subsequently the composition of the geopolymer can also be calculated.

III. Bulk Chemical Analysis using XRF

It is not the aim of this paper to describe all relevant analytical techniques, but it is worth providing some details about x-ray fluorescent spectroscopy as it is commonly used in conjunction with XRD [6,7,9,16]. When x-rays are directed onto a sample, one outcome is the emission of an electron from an inner orbital. The excited atom may relax by an electron in a higher orbital dropping back to the lower orbit and in so doing emitting a photon (x-ray) equal to the energy difference between the two orbitals. As each atom has a unique set of orbital energies it is possible to identify the atom in the sample by measuring the energy of the emitted photons. XRF is thus capable of identifying the elemental composition of a sample but cannot be used to extract crystallographic or phase information. Results from mineral-based samples are typically reported as oxide weight percentage based on stoichiometry. Sometimes this is misleading as Si may be present in fly ash as quartz (SiO_2), mullite ($3Al_2O_3$-$2SiO_2$) and amorphous, but what is reported is the total Si as SiO_2. As XRF cannot identify the source of the Si, it is important to combine information from XRD and XRF so that a comprehensive understanding of sample composition can be obtained.

IV. Supporting Characterisation Techniques

There are many other techniques that provide important information about precursors and resultant geopolymers. Two of note that will be mentioned here are particle size and morphological characterisation. Particle size is commonly measured using laser diffraction sizing, providing particle size distribution and surface area. For more accurate surface area assessment, the BET technique is usually adopted. Particle size and shape can be assessed in scanning electron microscopes (SEM) with considerable accuracy, however, to analyse a statistically significant number of particles, multiple x-ray-detector-based SEM should be used.

(1) Case study 1: Effect of precursor composition on strength development

The following example demonstrates the need to thoroughly characterise fly ash as a geopolymer precursor. The bulk elemental composition provided by XRF (Table 1) indicates suitable levels of aluminosilicates, but does not reveal the amount of reactive Si and Al. The overall Si:Al of 1.62 could be expected to produce a suitable geopolymer, although XRD analysis reveals much of the Si is locked in unreactive phases of quartz and mullite.

Table 1: Typical XRF analysis (wt%) of the main elements expressed as oxides and loss on ignition of fly ash from Collie power station in Western Australia. Note that the total molar Si:Al value at the bottom of the table.

SiO_2	51.38
Al_2O_3	26.90
Fe_2O_3	13.20
CaO	1.70
LOI	0.44
Si:Al molar	1.62

Table 2 shows the quantitative XRD result from the same fly ash batch. Of interest is that almost 42 wt% is crystalline quartz and mullite, which strongly influence the Si:Al obtained from the sample by means of XRF. It is these phases that need to be excluded from any assessment of the reactive Si:Al value of the fly ash. Also of interest is that two quartz phases have been determined to be present in the sample. The primary quartz is the original quartz in the coal that has come through the coal burning process intact. This quartz has a relatively large particle size and is usually not associated with the spherical fly ash spheres. The secondary quartz arises from dissociation of clay impurities in the coal (Equation 1) with considerably smaller particle size than the primary quartz and is typically embedded in the fly ash spheres. As shown in Equation 1, the clay dissociates into mullite and quartz.

Table 2: Quantitative XRD results (wt%) from the same ash in Table 1.

Primary quartz	15.05
Secondary quartz	11.14
Mullite	15.80
Fe_3O_4	2.51
Fe_2O	1.50

$$3(Al_2O_3{\cdot}2SiO_2) \rightarrow 3Al_2O_3{\cdot}2SiO_2 + 4SiO_2 \qquad (1)$$

The two quartz components can be differentiated in XRD patterns because they have small but measurable differences in their d-spacings. If now the XRF and XRD

results are combined, it is possible to calculate the composition of the amorphous component and thus its Si:Al (Table 3). The Si:Al of the reactive component is 1.15, considerably lower than the 1.62 obtained from XRF alone. Surprisingly, the reactive component has a relatively high Fe content that has been found to not react or impinge on the geopolymerisation process [16].

Table 3: Composition of amorphous component in Collie fly ash (wt%) determined from XRF (Table 1) and XRD (Table 2). Note the molar Si:Al value of the amorphous component.

SiO_2	20.90
Al_2O_3	15.39
Fe_2O_3	9.11
CaO	1.74
Si:Al molar	1.15

The Si:Al difference between the whole sample and amorphous component is even more dramatic for other Australian fly ashes (Table 4), with Tarong exhibiting a 217-% increase relative to the whole sample value. The variations in Si:Al shown in Table 4 drive home the point that if details about the composition of the amorphous (reactive) component are not known, it is impossible to develop a sensible geopolymer formulation. In fact for Tarong the alkali activator needs to be changed from a sodium silicate to a sodium aluminate if practical Si:Al values are to be achieved.

Table 4: Si:Al values for fly ash from three different power stations in Australia (Rickard et al 2011).

Fly ash source	Si:Al molar – whole Sample [XRF]	Si:Al molar – amorphous
Collie	1.62	1.15
Eraring	2.42	4.98
Tarong	2.79	8.84

Williams and van Riessen [6] conducted an experiment where geopolymer was made using Si:Al of the bulk sample and then the amorphous component (Table 5). As predicted, use of the Si:Al of the amorphous component resulted in a dramatic improvement in compressive strength. It is worth noting that the modest strength values obtained were the result of using constrained ratios to keep the comparison between different source fly ashes valid.

For some fly ashes, knowledge of the Si:Al of the amorphous component is sufficient to work out a geopolymer formulation for targeted Si:Al values. Collie fly ash is an example; compressive strength values of 130 MPa have frequently been achieved [17]. This was largely due to the amorphous component being concentrated on the surface of the fly ash spheres and thus readily accessible to the alkali for dissolution [16]. This is not always the case as power station operating parameters as well as the coal source may result in the amorphous component being trapped inside the fly ash spheres. In this situation the only way to achieve reproducible geopolymer products is to first mill the ash. This extra step is not always feasible as it introduces additional costs and increases the amount of water required for acceptable workability owing to loss of the uniform fly ash spheres.

Table 5: The average compressive strength (MPa) of the geopolymers samples made according to Si:Al determined for bulk and amorphous component of fly ash (Williams et al (2011).

Fly ash source	Bulk composition	Amorphous composition
Collie	7(3)	29(7)
Port Augusta	24(8)	48(12)
Bayswater	-#	9.5(12)
#Too fragile to test		

(2) Case study 2: Measuring the proportion of reacted aluminosilicate precursor

The challenge in producing high-quality geopolymers is to achieve targeted compositional ratios so that properties match the end use of the product. This may appear to be straightforward if starting with a stoichiometric aluminosilicate and alkali with known composition. In fact, the actual compositional ratios may be alarmingly different from targeted values, resulting in unexpected poor mechanical properties. This may be surprising if the starting material is well known. Upon closer inspection it becomes obvious that rarely does all of the aluminosilicate completely dissolve (Fig. 2). This need not be a big problem except that the final product is a mixture of geopolymer and residual precursors. However, if the amount of reacted precursor (aluminosilicate) is not known then the compositional ratios of the geopolymer are also not known with the concomitant problem that physical properties of the geopolymer are unpredictable. It is worth investigating why it is that when precursors such as metakaolin and sodium silicate are mixed the outcome can be so different than expected.

It could be as simple as inadequate mixing. This could be insufficient mixing time and/or use of a low-shear mixer that cannot break up the aluminosilicate so it is exposed to the alkali. If mixing is not a problem then an incorrect liquid-to-solid ratio could also be the cause. Rather than dwell on mixing or formulation issues for the moment, it is worth pointing out that the geopolymerisation process also plays a role in preventing dissolution of all the solid precursor. Dissolved Si and Al species rapidly form SiO_4 and AlO_4^- monomers, which in turn polymerise to form geopolymer. If the geopolymer forms on the surface of unreacted metakaolin then further dissolution is prevented

from occurring. The microstructure of metakaolin can impede dissolution because it is difficult for alkali to penetrate its platy structure. In fact, use of metakaolin dictates the use of higher liquid-to-solid ratios to achieve adequate mixing, while for fly ash the liquid-to-solids ratio can be lower as the spherical morphology of the ash makes it easier to mix. However, if a large proportion of the reactive part of the fly ash is embedded in the spheres then normal mixing procedures will be unsuccessful. It will be necessary to mill the fly ash first so the alkali can gain access to the reactive component.

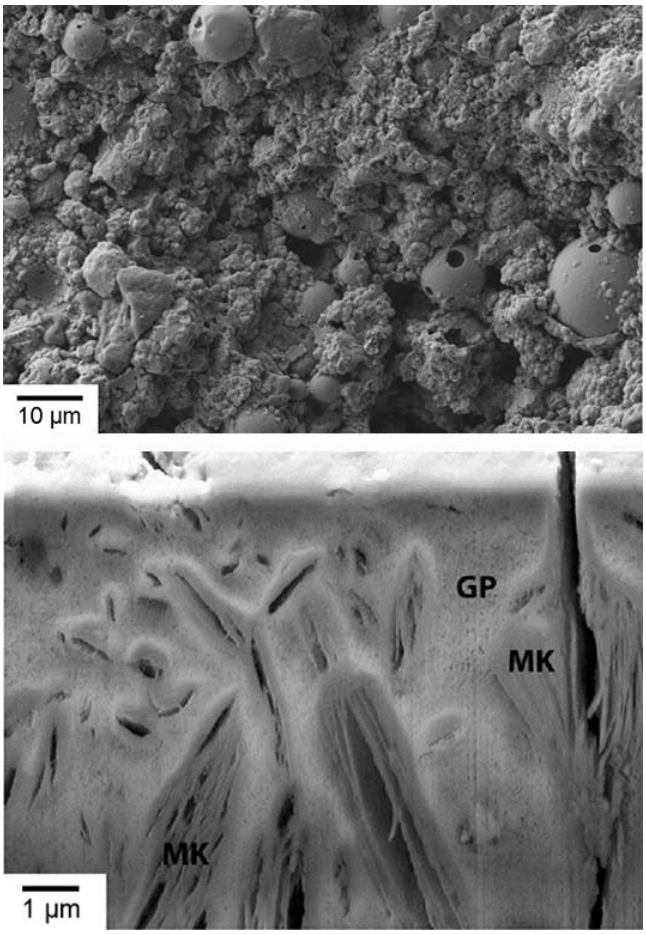

Fig. 2: SEM images of fly ash (left) and MK-based (right) geopolymer showing presence of unreacted precursor.

Several researchers [16,17,18] have set out to follow the precursor dissolution process by measuring dissolution after a series of set times, say 15 minutes apart. Periodically stopping the experiment and measuring the degree of dissolution with XRD and/or SEM is a slow process and generally limits the level of geopolymerisation because excess alkali is being used. These experiments are useful but unable to provide a complete picture of what happens after dissolution.

Being aware that not all the reactive precursor reacts during alkali dissolution and geopolymerisation is helpful in understanding the final properties of the geopolymer, however, it is important to be able to quantify the extent of reaction as part of the microstructural characterisation. Williams *et al.* [9] used four methods to determine the extent of reaction of metakaolin-based geopolymers; two methods were based on SEM and two methods used XRD. A summary of the approach and outcomes is provided below; complete details can be obtained from Williams *et al.* [9].

Four metakaolin-geopolymer samples were made using a targeted range of Si:Al, Na:Al and H:Si values (related to water:solids ratio) (Table 6). After seven days, compressive strength was measured and samples were then crushed so that the amount of reacted metakaolin could be determined.

X-ray diffraction methods

Method 1: XRD-Area Ratio Method (ARM)

This approach is similar to the standard addition method used extensively in chemistry.

Method 2: XRD-Partial or No Known Crystal Structure (PONKCS)

The PONKCS method [15] requires a sample with 100 % of the phase with unknown structure (metakaolin).

Scanning electron microscope methods

EDS: X-ray spectra were calibrated against well-characterized kaolinite and feldspar samples covering the range of sodium, aluminium, and silicon observed in these samples.

Table 6: Target compositions and compressive strengths of the samples prepared for determination of amount of reacted metakaolin. Values in parentheses correspond to the least significant figure in the standard deviation to the left.

Sample No.	Si:Al	Na:Al	H:Si	Compressive strength (MPa)
1	1.92	1.00	5.53	67(17)
2	2.50	1.26	6.09	33(6)
3	3.08	1.53	5.94	3.1(2)
4	1.55	1.07	6.47	14(4)

Point counting analysis

SEM images of the samples were collected to enable point counting to be used to determine the unreacted metakaolin in the geopolymer matrix using a procedure modified from ASTM C 1356 M [19].

A qualitative inspection of the XRD patterns reveals obvious differences between the precursor metakaolin and geopolymer samples both in position of the amorphous hump and its shape. The geopolymer samples also reveal differences in their shape and peak position. It should be noted that sharp reflections in the patterns are from quartz (Fig. 3).

Calculation of the fraction of reacted metakaolin from the two XRD methods and SEM point counting is presented in Table 7. The results are relatively close, considering the differences in the methods. Geopolymer Samples 1 and 4 with Si:Al of 1.92 and 1.55, respectively have the highest proportion of reacted metakaolin but a dramatic

difference in strength (Sample 1: 67 MPa and Sample 4: 14 MPa). On face value this suggests that the amount of reacted metakaolin is not the only relevant factor in controlling strength though further analysis reveals additional information.

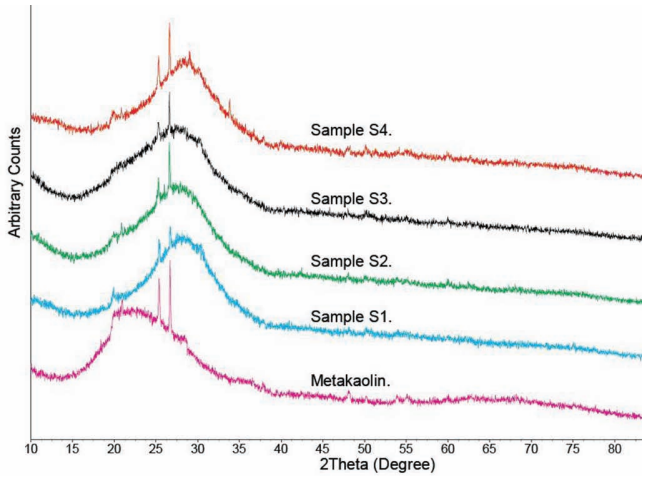

Fig. 3: XRD patterns of the precursor metakaolin and four geopolymer samples. Patterns have been offset in the vertical direction for clarity.

Table 7: Fraction of reacted metakaolin from XRD and SEM. Values in parentheses corresponds to the least significant figure in the standard deviation to the left.

Sample no.	XRD (ARM)	XRD (PONKCS)	SEM (point counting)
1	71(1)	69.2(5)	70(1)
2	52(2)	47.4(6)	52(2)
3	10(8)	3.3(6)	12(4)
4	75(3)	80.8(4)	81(1)

In addition, for determination of the reacted component of metakaolin it is also possible to calculate the composition of the geopolymer matrix and thus estimate Si:Al. Table 8 shows the targeted Si:Al as well as the measured values from the four methods. For Samples 1 and 4 the bulk and measured values are comparable while for Sample 2 the x-ray methods and SEM method are 50 % higher than the bulk value. For Sample 3 the measured values range from six times to 17 times greater than the bulk value.

The results presented in Table 8 can be used to explain why there is such a large variation in compressive strength between different samples. Sample 3 was very weak (compressive strength of only 3.1 MPa) because only a small fraction of the precursor metakaolin reacted, resulting in a small amount of binder. When only a small proportion of metakaolin reacts, the geopolymer binder that forms is automatically low in Al, creating high-Si:Al and -Na:Al material that is intrinsically weak.

Williams *et al.* [9] introduced robust and useful methods for analysing differences in both the amount of geopolymer binder and its composition. Their experiment revealed that while the amount of geopolymer is important, it is dominated by the need to have the correct range of Si:Al and Na:Al to achieve high-strength samples.

Table 8: Si:Al of targeted (bulk) geopolymer compared to measured values.

Sample no.	Bulk Sample	XRD (ARM)	XRD (PONKCS)	SEM (point counting)	EDS
1	1.92	2.28	2.26	2.29	2.09
2	2.50	3.84	3.98	3.84	2.81
3	3.08	20.6	51.95	17.52	-
4	1.55	1.72	1.66	1.67	1.74
Note: The accuracy of the EDS data was limited for Sample 3 owing to the very small regions of geopolymer dispersed throughout the microstructure.					

When starting work with a new aluminosilicate precursor, it is desirable to make a series of samples with different ratios to determine the optimum ratios. However, this approach is not fool-proof; as mentioned previously it maybe that a fly ash precursor needs to be milled or sieved before adequate strength values can be achieved. Thus a multitude of samples can be made in the hope of striking a combination that produces a geopolymer sample with the correct specifications or a rigorous characterisation process can be undertaken to derive a formulation to achieve targeted outcomes.

The above scientific approach is deemed necessary for a comprehensive understanding of the critical parameters essential in making high-quality geopolymer products. However, the approach outlined looks only at the starting precursor(s) and final product (geopolymer and unreacted precursor), with no investigation into the path between the two. Tracking the precursor dissolution and subsequent polycondensation allows the kinetics of the processes to be obtained. However, measurements using the x-ray characterisation methods discussed so far are too slow using laboratory sources. High-brightness x-ray beams from synchrotron radiation sources are required to enable rapid acquisition of XRD patterns over many hours.

(3) Case study 3: Monitoring extent of reaction using in situ synchrotron-based XRD

The high brightness of the synchrotron beam enables diffraction patterns to be obtained in only a few minutes so that sequential patterns can be collected over several hours. In fact, with a specially designed sample holder, sequential patterns can be collected from several samples. Provis and van Deventer [20, 21] used synchrotron-based energy-dispersive XRD to performed such an experiment and tracked the "extent of reaction", but the sensitivity and modelling method was such that the amorphous precursor and geopolymer components could not be independently quantified. Williams and van Riessen [22] conducted an experiment using wavelength-dispersive XRD, with

higher resolution, at the Australian synchrotron and were able to model both unreacted precursor and geopolymer simultaneously along with crystalline phases. Data collection times were a few seconds per pattern per sample, so many 10s of samples could be analysed simultaneously. The basis of this experiment was to mix aluminosilicate precursors and alkali, place the slurry in a 1.5-mm I.D. polyetheretherketone (PEEK) tube, seal the tube and place it in the sample holder of a beamline set up for high-resolution XRD (Table 9).

Table 9: Target compositions and compressive strengths of samples prepared for in situ synchrotron-based XRD.

Sample	Si:Al	Na:Al	H:Si	Compressive strength (MPa)
1	1.8	0.8	5.5	14(2)
2	2.0	0.8	5.5	35(3)
3	2.0	1.2	5.5	50(9)
4	2.2	0.8	5.5	40(7)

Two-dimensional XRD patterns (not shown here) consisted of sharp rings from crystalline phases and diffuse rings from amorphous phases. Crystalline phases consisted of mullite, quartz (secondary) and iron oxides originally from the fly ash and zeolite-like phases (Sample 1, Table 9) formed after mixing of fly ash and alkali. The sharpness of the crystalline ring patterns indicates they arose from large numbers of small crystallites. Rings from the amorphous phases were observed to increase in diameter with time. A spot pattern from primary quartz was found to be superimposed on the ring pattern, indicating the source was from a low number of large crystallites in the beam. The presence of primary and secondary quartz is consistent with findings of Williams and van Riessen [6]. Of interest is that at the beginning of the experiment the spots moved position radially on the ring between patterns and then after a period of time stopped. This cessation of spot movement was ascribed to the initial setting of the geopolymer binder that spatially locked in the primary quartz. Table 10 shows how setting time varied for the four samples. Although the setting time was not verified separately by, for example, using a Vicat needle in an identical sample, it demonstrates the potential for using this approach as an independent method for assessing the time when the sample loses plasticity. There were two distinct unidentified zeolites that formed in Sample 1. The first zeolite, after an induction time (~1.4 h), rapidly increases in concentration and crystallite size (determined using the integral breadth method) to a plateau value (Fig. 4). This suggests that this phase increases concentration via crystal growth. The second zeolite phase exhibited a long induction period (~12 h) and showed different formation behaviour. The crystallite size instantaneously increases to a plateau value, then the concentration increases while the crystallite size decreases, indicating that the crystal growth rate is much faster than the nucleation rate for this second zeolite (Fig. 5). Presentation of the diffraction data time series as a 2D colour contour image (Fig. 6), where intensity is shown by colour scale, reveals information about evolution of the phases just discussed.

An example of the extensive range of information that can be extracted from time-resolved data is shown in Fig. 7, where both dissolution of fly ash and formation of geopolymer are shown along with the two zeolites phases. Also included in Fig. 7 is the Power Law pre-factor which is proportional to the low-angle intensity in the diffraction patterns, and is a normalisation of a parameter in the equation used to refine the background of the x-ray diffraction pattern [23]. The Power Law pre-factor is correlated to the specific surface area of the sample, so in this case indicates the presence of very small particles. For Sample 4, the fly ash dissolution occurs consistently for about 5 h; well beyond the initial setting time of 64 min. When the dissolution rate plateaus, 42 % of the amorphous component of the fly ash had dissolved. Dissolution and polycondensation occurred synchronously so that as dissolution halts the formation of geopolymer plateaus. The area bounded by the Power Law pre-factor curve and geopolymer curve from when the geopolymer curve is between 10 % and 75 % provides a strong correlation with compressive strength (Fig. 8). In addition, Fig. 9 shows there is a strong correlation, over a limited range, between the compressive strength of the samples and the standard deviation of the H:Si ratio during formation of the geopolymer

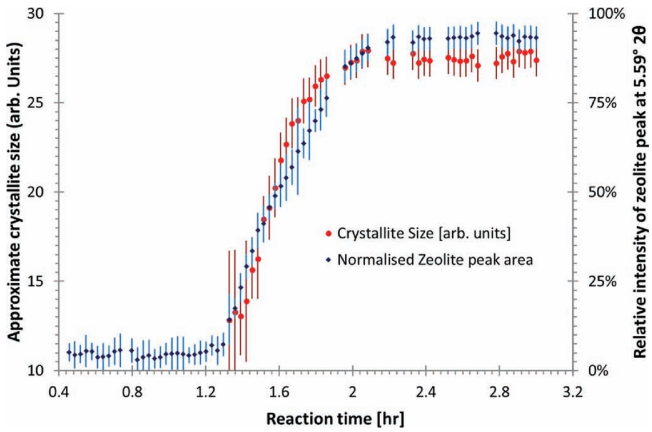

Fig. 4: Evolution of zeolite phase 1 with time. Also shown is change in crystallite size with time.

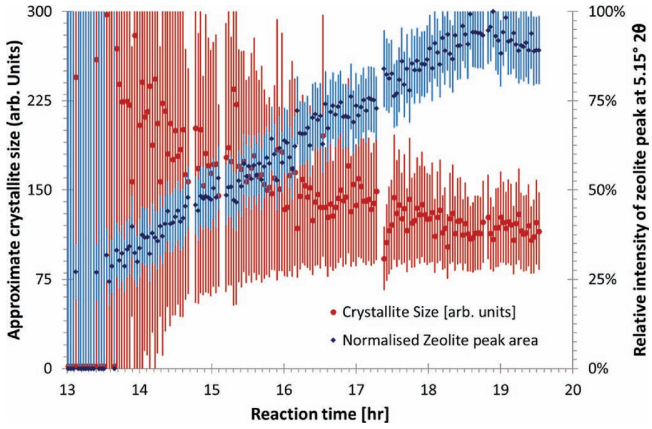

Fig. 5: Evolution of zeolite phase 2 with time. Also shown is change in crystallite size with time.

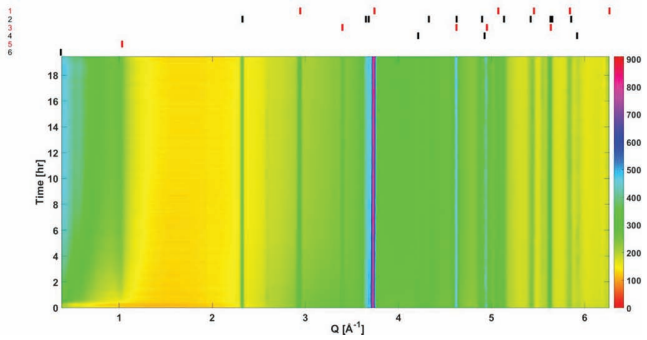

Fig. 6: Time resolved diffraction pattern of Sample 3. Features include the evolution of low angle intensity (<1 Å^{-1}) and the 'shift' in the amorphous peak position (deep yellow). The peak positions of significant identified phases are shown at the top of the figure for [1] Quartz (SiO_2), [2] Mullite ($Al_{4.64}5Si_{1.36}O_{9.68}$), [3] Hematite ($Fe_2O_3$), [4] Magnetite ($Fe_3O_4$) and [5] unspecified zeolite and [6] small angle scattering.

Table 10: Setting time of geopolymer samples based on when primary quartz spots stopped moving in XRD patterns.

Sample	Setting time (min)
1	24
2	25
3	32
4	64

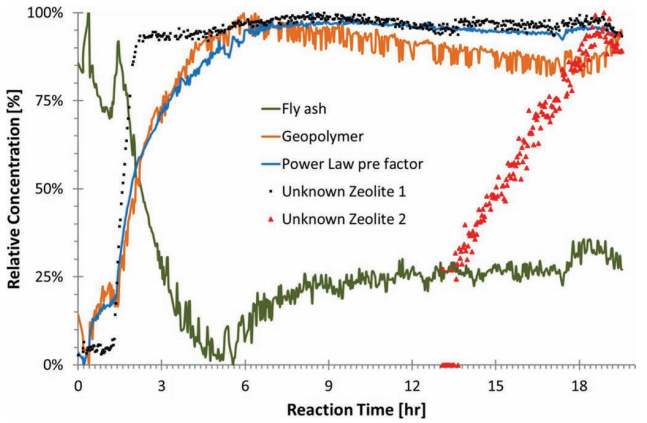

Fig. 7: XRD data for Sample 4 showing dissolution of fly ash and formation of geopolymer along with two zeolite phases. The Power Law pre-factor is included for comparison.

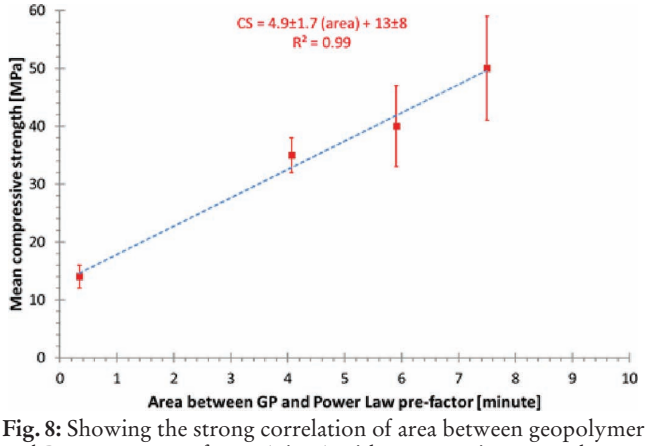

Fig. 8: Showing the strong correlation of area between geopolymer and Power Law pre-factor (Fig. 5) with compressive strength.

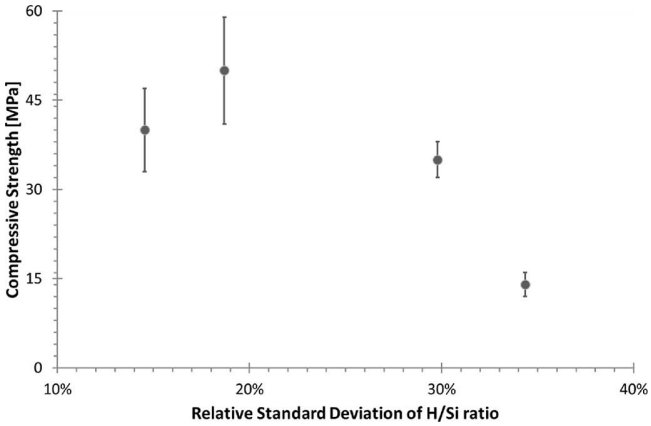

Fig. 9: Correlation between compressive strength and relative standard deviation of H:Si ratio.

(4) Case study 4: In situ XRF and scanning x-ray diffraction microscopy

The use of *in situ* XRD as described earlier provides a plethora of information about precursor dissolution and geopolymer formation. The effect of changes in precursor composition, mix formulation or curing regime on the geopolymerisation process can be directly and quantitatively assessed, thus allowing optimisation of the final geopolymer product. However, an approach that provides structural information averaged over the volume of the x-ray probe is inherently limited. The properties of geopolymers, their precursor materials, and even the geopolymer formation process are all closely related to their compositional and physical heterogeneity on length scales of micrometres and below. Scanning x-ray micro- and nanoprobe techniques using synchrotron radiation allow the local properties of materials with complex heterogeneity to be studied. Developments in nanofocussing optics and high-brightness light sources promise nanoscale resolution, but simultaneously achieving high elemental sensitivity and high spatial resolution usually requires a compromise in data acquisition time that may be incompatible with *in situ* observations of dynamic processes.

Synchrotron-based XRF microscopy (XFM) offers extremely high sensitivity for mapping the distribution of elements at a resolution determined by the incident probe size [24]. Scanning x-ray diffraction microscopy (SXDM) is a lensless imaging method that allows quantitative images of structures consisting of light elements to be obtained with spatial resolution that is not limited by the probe size. Diffraction patterns are collected from overlapping areas illuminated by a coherent probe and quantitative images of the sample are recovered using iterative approaches. This method is generally referred to as 'ptychography' [25]; SXDM is used to describe the special case in which the sample is positioned at the plane where an x-ray beam is focussed [26].

The various benefits of combining XFM and SXDM methods have recently been demonstrated [27,28]. In the present context, the dissolution of precursor material and polycondensation processes can be studied *in situ* by correlating the morphological and density changes observed with high resolution by means of SXDM with the local variations in elemental composition at micrometre

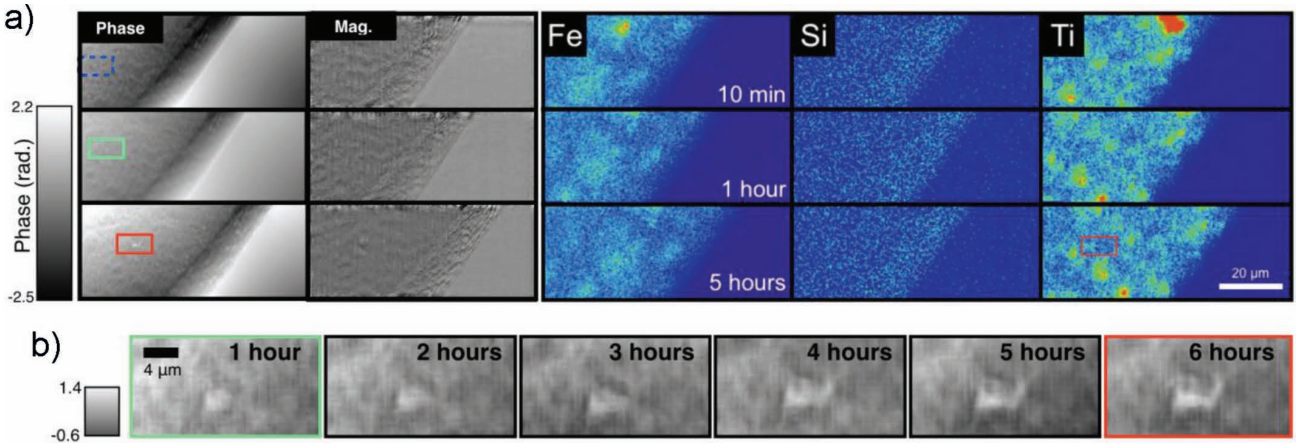

Fig. 10: SXDM and XFM images of geopolymer obtained simultaneously during curing. Metakaolin solid precursor and sodium silicate alkali solution were mixed and sandwiched between silicon nitride membranes. The greyscale maps show the phase and magnitude of the sample transmission function that was reconstructed from the SXDM data. The coloured maps show the distribution of selected elements (Fe, Si and Ti) by XFM. Data were obtained over a period of 6 hours and are presented in (a) without any correction for drift. The SXDM phase maps in (b) show the feature indicated in (a) after correcting for its displacement over the duration of the experiment to highlight that morphological changes on the sub-micrometre length scale can be recognised.

length scales by means of XFM. The quantitative absorption and phase contrast images provided by SXDM have previously been used to quantify variations in density in cement materials [29,30] by means of XFM. *In situ* applications of SXDM are receiving considerable attention with a wide variety of sample environments [31,32,33,34]. An overview of synchrotron-based techniques for characterisation of geopolymers by Provis *et al.* [12] concludes that future work is likely to be obtained by a combination of complementary techniques. This is seen in, for example, the recent work by Hu *et al.* [35,36] where nano XRF and nano tomography were used to measure the 3D structure of C_3S hydration.

The large-solid-angle, multi-element Maia detector system [37] at the XFM beamline at the Australian Synchrotron [38] allows rapid XFM imaging of large samples. A fast-framing single-photon-counting pixel detector (EIGER X 1M, Dectris, Ltd. Baden, Switzerland) for SXDM data acquisition allows the two methods to be performed simultaneously with continuous (on-the-fly) scanning [28]. We employed this approach in a pilot study to demonstrate the feasibility of combining SXDM and XFM for analysis of geopolymer formation. Alkali and solid precursor were mixed and sealed between two 100-nm-thick silicon nitride membranes. 10 keV x-rays were focussed to a spot of approximately 2.5 μm FWHM at the sample. The detector used to collect diffraction data was placed 3.67 m downstream of the focus. The fluorescence data were collected with the Maia detector placed in backscatter geometry. Data were collected from the same area of approximately 9000 μm^2 in intervals of approximately 6 min. 13 241 diffraction data frames were reconstructed for each image using the ePIE algorithm [38] with a reconstructed SXDM pixel size equal to 47.4 nm using a method similar to that described in Jones *et al.* [28].

The reconstructed SXDM images (phase and magnitude) are shown in Fig. 10, together with elemental maps for selected elements that were simultaneously obtained with XFM. In all images there is a clear delineation between the liquid alkali and solid metakaolin/geopolymer. The Ti and Fe maps can be used to track sample drift as they play no part in the geopolymerisation process. The XFM detection efficiency for the key elements in the reaction, namely Na, Al and Si, is very low. The SXDM images reveal considerable structure in the solid phase formed by these light elements. Even though the metakaolin/geopolymer was approximately 2 μm thick, the evolution in microscale features can be tracked in the SXDM phase maps (Fig. 10b) over a period of 6 h.

The XFM and SXDM data demonstrate the potential for *in situ* imaging with chemical, spatial and temporal information. Variations in Si concentration can potentially be used to follow dissolution/polycondensation if sensitivity can be improved (e.g. with a XRF detector optimised for low photon energy and longer acquisition times). In a follow-up experiment (not presented here) sodium silicate was replaced by caesium silicate to provide greater discrimination between the starting metakaolin and resultant geopolymer via the Cs fluorescence signal. With the use of a less dense distribution of metakaolin, the dissolution and condensation processes around individual particles of precursor material can be studied.

V. Conclusions

Here we have presented a workflow for geopolymer formulation development and microstructural analysis and have highlighted four case studies that outline the evolution of techniques that have contributed to a greater understanding of how to design and optimise a geopolymer. Initially precursors need to be thoroughly characterised before a geopolymer formulation is designed. Once a geopolymer has been made, it is necessary to determine what proportion of aluminosilicate precursor has reacted; this enables targeted ratios to be compared with actual ratios. If there is a discrepancy between the targeted and actual ratios, there may be a need to beneficiate the precursor and/or alter the alkali to enable the geopolymer to reach expected physical properties such as strength. Characterising the geopolymer sample after curing provides considerable insight into the reaction between aluminosilicate

precursor and alkali but does not reveal the processes that occurred during dissolution and polycondensation. *In situ* synchrotron-based XRD techniques provide the means to track the dissolution rates and geopolymer formation rates as well as delivering a means to measure setting time. *In situ* XRD methods are important but are limited in their spatial discrimination, which can be partially overcome with *in situ* synchrotron-based XRF and SXDM. Although their full potential is yet to be realised, these techniques offer means of directly imaging dissolution and polycondensation in addition to revealing diffusion rates and lengths. It is obvious that the in-depth approach outlined in this paper cannot be repeated for every combination of precursor and alkali, but where it is important to optimise a geopolymer for a particular application it would be prudent to do so.

The following points summarise the conclusions drawn from the work presented in this paper;

- Quantifying precursor materials is crucial for informed mix design and reduces 'trial and error'
- A combination of XRD and XRF analysis allows for the reactive composition of the source material to be determined
- Particle size and morphology analysis allows for an understanding of reactive surface area and water requirements of the mix formulation
- Comparison of the composition of the formed geopolymer binder with the designed composition allows for the extent of reaction to be assessed
- Precursors can be beneficiated by means of milling or activator composition can be altered to optimise formulation. Curing conditions are also important
- *In situ* experiments enable the geopolymerisation reaction to be monitored, providing a better understanding of curing conditions and therefore aiding in the optimisation of physical properties. Specifically, it has been possible to:
  - Confirm that there are multiple mechanisms of zeolite formation even within the same geopolymer sample.
  - Identify a new method to separately measure the feedstock dissolution and geopolymer formation progress *in situ*, which will allow a large number of optimisation experiments to be completed in the future.
  - Identify significant temporal variations in the composition of the solution from which the geopolymer forms; the relative standard deviation of the H:Si ratio during formation correlated with the physical properties.
  - Derive a new method, albeit time consuming, to measure the setting time of geopolymer paste formation.
  - The XFM and SXDM data demonstrate the potential for *in situ* imaging of precursor/geopolymer systems with chemical, spatial and temporal information.

Acknowledgements

Part of this research was undertaken on the XFM beamline at the Australian Synchrotron, Victoria, Australia, and supported by the Multi-modal Australian ScienceS Imaging and Visualization Environment (MASSIVE) (http://www.massive.org.au). Nicholas Phillips, Michael Jones and Martin de Jonge are thanked for their support during XFM/SDXM data collection. Nigel Chen-Tan's contribution to development of geopolymer technology at Curtin is acknowledged.

References

1 Roy, D.M.: Alkali-activated cements. opportunities and challenges, *Cement Concrete Res.*, **29**, 249 – 254, (1999).

2 Shi, C., Krivenko, P.V., Roy, D.: Alkali-activated cements and concretes. Taylor and Francis, Milton Park, 2006.

3 Provis, J.L., van Deventer, J.S.J.: Geopolymers: Structure, processing, properties and industrial applications. Woodhead Publishing Limited, Oxford, 2009.

4 Glasby, T., Day, J., Genich, R., Kemp, M.: Commercial scale geopolymer concrete construction, In: Proceedings of the saudi international building and constructions technology conference, 2015.

5 van Riessen, A., Chen-Tan, N., Portella, J., Bernard, J.S., Gourley, T.: Chapter 14: Geopolymer Cement and Concrete, 441 – 458. In Coal Combustion Products Handbook – Second Edition. Editors: Ward, C., Heidrich, C., Yeatman, O.: Ash Development Association of Australia, (2014).

6 Williams R., van Riessen, A.: Determination of the reactive component of fly ashes for geopolymer production using XRF and XRD, *Fuel*, **89**, 3683 – 3692, (2010).

7 Rickard, W.D.A., Williams, R., Jadambaa T., van Riessen, A.: Assessing the suitability of three australian fly ashes as an aluminosilicate source for geopolymers in high temperature applications, *Mat. Sci. Eng. A*, **528**, 3390 – 3397, (2011).

8 Cement Industry Federation, Cementing Our Future 2005 – 2030. Technology Pathway for the Australian Cement Industry, 2005

9 Williams, R., Hart, R., van Riessen, A.: Quantification of the extent of reaction of metakaolin based geopolymers using XRD, SEM and EDS, *J. Am. Ceram. Soc.*, **94**, [8], 2663 – 2670, (2011).

10 Sturm, P., Greiser, S., Gluth, G.J.G., Jäger, C., Brouwers, H.J.H.: Degree of reaction and phase content of silica-based one-part geopolymers investigated using chemical and NMR spectroscopic methods, *J. Mater. Sci.*, **50**, 6768 – 6778, (2015).

11 van Riessen, A., Chen-Tan, N.: Beneficiation of collie fly ash for synthesis of geopolymer, part 1 – beneficiation, *Fuel*, **106**, 569 – 575 (2013a).

12 Provis, J.L., Hajimohammadi, A., White, C.E., Bernal, S.A., Myers, R.J., Winarski, R.P., Rose, V., Proffen, T.E., Llobet, A., van Deventer, J.S.J.: Nanostructural characterization of geopolymers by advanced beamline techniques, *Cement Concrete Comp.*, **36**, 56 – 64, (2013).

13 Liu, X., Aranda, M.A.G., Chen, B., Wang, P., Harder, R., Robinson, I.: In Situ Bragg Coherent Diffraction Imaging Study of a Cement Phase Microcrystal during Hydration, Cryst. Growth Des., 15, [7], 3087 – 3091, (2015).

14 Rietveld, H.M.: A profile refinement method for nuclear and magnetic structures, *J. Appl. Crystallogr.*, **2**, 65 – 71, (1969).

15 Scarlett, N.V.Y., Madsen, I.C.: Quantification of phases with partial or no known crystal structures, *Powder Diffr.*, **21**, 278 – 284, (2006).

16 Chen-Tan, N.W., van Riessen, A., Ly, C.V., Southam, D.C.: Determining the reactivity of a fly ash for production of geopolymer, *J. Am. Ceram. Soc.*, **92**, [4] 881 – 887, (2009).

17 Chen-Tan, N.W.: Geopolymer from a western australian fly ash, PhD Thesis, Curtin University (2010).

[18] Fernández-Jiménez, A., Palomo, A., Criado, M.: Microstructure development of alkali-activated fly ash cements: a descriptive model, *Cement Concrete Res.*, **35**, 1204 – 1209, (2005).

[19] ASTM C 1356 M. Standard Test Method for Quantitative Determination of Phases in Portland Cement Clinker by Microscopical Point-Count Procedure, (2001).

[20] Provis, J.L., van Deventer, J.S.J.: Geopolymerisation Kinetics. 1. in situ energy dispersive x-ray diffractometry, *Chem. Eng. Sci.*, **62**, 2309 – 2317, (2007).

[21] Provis, J.L., van Deventer, J.S.J.: Geopolymerisation Kinetics. 2. reaction kinetic modelling, *Chem. Eng. Sci.*, **62**, 2318 – 2329, (2007).

[22] Williams R., van Riessen, A.: The first 20 hours of Geopolymerization: an in situ WAXS study of fly Ash-based geopolymers, *Materials*, **9**, 552, (2016).

[23] Williams, R.: Optimising geopolymer formation. PhD thesis, Curtin University, Perth, Western Australia (2015).

[24] Jones, M.W.M., de Jonge, M.D., James, S.A., Burke, R.: Elemental mapping of the entire intact drosophila gastrointestinal tract, *J. Biol. Inorg. Chem.*, **20**, 979 – 987, (2015).

[25] Rodenburg, J.M., Hurst, A.C., Cullis, A.G., Dobson, B.R., Pfeiffer, F., Bunk, O., David, C., Jefimovs, K., Johnson, I.: Hard-X-Ray Lensless Imaging of Extended Objects, Phys. Rev. Lett., 98, [3], 034801 (2007).

[26] Thibault, P., Dierolf, M., Menzel, A., Bunk, O., David, C., Pfeiffer, F.: High-resolution scanning x-ray diffraction microscopy, Science, 321, 379 – 382, (2008).

[27] Deng, J., Vine, D.J., Chen, S., Nashed, Y.S.G., Peterka, T., Ross, R., Jacobsen, C.J.: Opportunities and limitations for combined fly-scan ptychography and fluorescence microscopy. In X-Ray Nanoimaging: Instruments and Methods II (Vol. 9592) (2015). [95920U] SPIE. doi: 10.1117/12.2190749

[28] Jones, M.W.M., Phillips, N.W., van Riessen, G.A., Abbey, B., Vine, D.J., Y.S.G. Nashed, Y.S.G., Mudie, S.T., Afshar, N., Kirkham, R., Chen, B., Balaur E., de Jonge, M.D.: Simultaneous x-ray fluorescence and scanning x-ray diffraction microscopy at the australian synchrotron XFM beamline, *J. Synchrotron Rad.*, 23, 1151 – 1157, (2016).

[29] Trtik, P., Diaz, A., Guizar-Sicairos, M., Menzel, A., Bunk O.: Density mapping of hardened cement paste using ptychographic x-ray computed tomography, *Cement Concrete Comp.*, **36**, 71 – 77, (2013).

[30] da Silva, J.C., Trtik, P., Diaz, A., Holler, M., Guizar-Sicairos, M., Raabe, J., Bunk, O., Menzel, A.: Mass density and water content of saturated never-dried calcium silicate hydrates, *Langmuir*, **31**, 3779 – 3783, (2015).

[31] Baier, S., Damsgaard, C., Scholz, M., Benzi, F., Rochet, A., Hoppe, R., Grunwaldt, J.: In situ ptychography of heterogeneous catalysts using hard X-Rays: high resolution imaging at ambient pressure and elevated temperature, *Microsc. Microanal.*, **22**, [1], 178 – 188, (2016).

[32] Esmaeili, M., Floystad, J.B., Diaz, A., Høydalsvik,K., Guizar-Sicairos, M., Andreasen, J.W., Breiby, D.W.: Ptychographic X-ray tomography of silk fiber hydration, *Macromolecules*, **46**, 434 – 439, (2013).

[33] Høydalsvik, K., Floystad, J.B., Zhao, T., Esmaeili, M., Diaz, A., Andreasen, J.W., Mathiesen, R.H., Ronning M., Breiby, D.W.: In situ x-ray ptychography imaging of high-temperature CO_2 acceptor particle agglomerates, *Appl. Phys. Lett.*, **104**, 241909/1-5, (2014).

[34] Kourousias, G., Bozzini, B., Gianoncelli, A., Jones, M.W.M., Junker, M., van Riessen, G., Kiskinova, M.: Shedding light on electrodeposition dynamics tracked in situ via soft x-ray coherent diffraction imaging, *Nano Research*, **9**, [7], 2046 – 2056, (2016).

[35] Hu, Q., Aboustait, M., Kim, T., Tyler Ley, M., Hanan, J.C. Bullard, J., Winarski, R., Rose, V.: Direct three-dimensional observation of the microstructure and chemistry of C_3S hydration, *Cement Concrete Res.*, **88**, 157 – 169, (2016a).

[36] Hu, Q., Aboustait, M., Kim, T., Tyler Ley, M., Bullard, J.W., Scherer, G., Hanan, J.C., Rose, V., Winarski, R., Gelb, J.: Direct measurements of 3D structure, chemistry and mass density during the induction period of C_3S hydration, *Cement Concrete Res.*, **89**, 14 – 26, (2016b).

[37] Siddons, D.P., Kirkham, R., Ryan, C.G., De Geronimo, G., Dragone, A., Kuczewski, A.J, Li, Z.Y., Carini, G.A., Pinelli, D., Beuttenmuller, R., Elliott, D., Pfeffer, M., Tyson, T.A., Moorhead, G.F., Dunn, P.A.: Maia x-ray Microprobe Detector Array System, J. Phys. Conf. Ser., 499, 012001, (2014).

[38] Paterson, D., de Jonge, M.D., Howard, D.L., Lewis, W., McKinlay, J., Starritt, A., Küsel, M., Ryan, C.G., Kirkham, R., Moorhead, G., Siddons, D.P.: The X-ray Fluorescence Microscopy Beamline at the Australian Synchrotron, AIP Conf. Proc., 1365, 219 – 222, (2011).

[39] Maiden, A.M., Rodenburg, J.M.: An improved ptychographical phase retrieval algorithm for diffractive imaging, Ultramicroscopy, 109, [10], 1256 – 1262, (2009).